

A Bayesian Non-linear State Space Copula Model to Predict Air Pollution in Beijing

Alexander Kreuzer^{*†}, Luciana Dalla Valle[†] and Claudia Czado[†]

Technische Universität München[†] and University of Plymouth[†]

September 5, 2022

Abstract

Air pollution is a serious issue that currently affects many industrial cities in the world and can cause severe illness to the population. For this reason, a correct estimation and prediction of airborne pollutant concentrations is crucial. In this paper, we analyze hourly measurements of fine particulate matter and meteorological data collected in Beijing in 2014. We show that the standard state space model, based on Gaussian assumptions, does not allow to correctly capture the time dynamics of the observations. Therefore, we propose a novel non-linear non-Gaussian state space model where both the observation and the state equations are defined by copula specifications, and we perform Bayesian inference using the Hamiltonian Monte Carlo method. The proposed copula state space approach is very flexible, since it allows us to separately model the marginals and to accommodate a wide variety of dependence structures in the data dynamics. We show that the proposed approach allows us not only to accurately predict particulate matter measurements, but also to capture unusual high levels of air pollution, which were not detected by measured effects.

1 Introduction

Over recent decades, rapid economic development and urbanization lead to severe and chronic air pollution in China, which is currently listed as one of the most polluted countries in the world. Exposure to ambient air pollution has been associated with a variety of adverse health effects, ranging from cardiovascular and respiratory illnesses, such as stroke and ischemic heart disease, to cancer and even death (Liang et al (2015)). It has been shown that air pollution increases mortality and morbidity and shortens life expectancy (World Health Organization (2013)), with heavy consequences in terms of health care and economy (Song et al (2017)). Outdoor PM2.5 has been established as the best metric of air pollution-related risk to public health (Liu et al (2017)). PM2.5 consists of fine particulate matter with aerodynamic diameters of less than 2.5 micrometers (μm). It has been estimated that in China, ambient PM2.5 was the first-ranking mortality risk factor in 2015 and exposure to this pollutant caused 1.1 million deaths in the same year (Cohen et al (2017)).

Fine particulate matter is a key driver of global health and therefore it is vital to accurately model and estimate the exposure to PM2.5, especially in areas of severe and persistent air pollution such as China and its biggest cities like Beijing. A correct estimation and forecast of air pollution is crucial for a realistic appraisal of the risks that airborne contaminants pose and for the design and implementation of effective environmental and public health policies to control and limit those risks (Shaddick et al (2018)).

Most of the contributions in the literature focus on modeling the observed concentrations of ambient air pollution. Sahu et al (2006) modeled fine atmospheric particulate matter data collected in the US using a Bayesian hierarchical spatio-temporal approach. Hao et al (2015) adopted a logistic regression to estimate associations between preterm birth and average pollutant concentrations in the US. Guo et al (2016) and Dominici et al (2002) used generalized

* Corresponding author: E-mail: a.kreuzer@tum.de

additive models to examine the health effects of ambient air pollution in China and in the US, respectively.

State space representations, in addition to modeling the observed concentrations of air pollution, allow us to obtain an estimate of underlying non-measured factors, which might be critical to assess pollution-related health risks.

1.1 Linear Gaussian state space models

State space models are dynamic statistical analysis techniques which assume that the state of a system at time t can only be observed indirectly through observed time series data (Durbin and Koopman (2000)). State space models contain two classes of variables, the unobserved state variables, which describe the development over time of the underlying system, and the observed variables (Durbin and Koopman (2002)). The univariate linear Gaussian state space model with continuous states and discrete time points $t = 1, \dots, T$ can be formulated as follows

$$Z_t = \rho_t^{obs} W_t + \sigma_t^{obs} \eta_t^{obs} \quad (1)$$

$$W_t = \rho_t^{lat} W_{t-1} + \sigma_t^{lat} \eta_t^{lat}. \quad (2)$$

Here, $(Z_t)_{t=1, \dots, T}$ is a random vector corresponding to the observations, $(W_t)_{t=1, \dots, T}$ is an unobserved state vector and η_t^{obs} and η_t^{lat} are independent disturbances, with $\eta_t^{obs} \sim N(0, 1)$ and $\eta_t^{lat} \sim N(0, 1)$ for $t = 1, \dots, T$. The quantities ρ_t^{obs} , ρ_t^{lat} , σ_t^{obs} and σ_t^{lat} are assumed to be known. It is also assumed that $W_0 \sim N(\mu_0^{lat}, (\sigma_0^{lat})^2)$, where μ_0^{lat} and σ_0^{lat} are generally known. Equation (1) is commonly referred to as the observation equation and it describes how the observed series depends on the unobserved state variables W_t and on the disturbances η_t^{obs} . Equation (2) is referred to as the state equation and it describes how these state variables evolve over time (Van den Brakel and Roels (2010)).

The linear Gaussian state space model can also be expressed as

$$Z_t | W_t \sim N(\rho_t^{obs} W_t; (\sigma_t^{obs})^2) \quad (3)$$

$$W_t | W_{t-1} \sim N(\rho_t^{lat} W_{t-1}; (\sigma_t^{lat})^2) \quad (4)$$

Typically, Kalman filter recursions are used for determining the optimal estimates of the state vector W_t given information available at time t (Durbin and Koopman (2012)). Other methods, such as Empirical Bayes was proposed by Koopman and Mesters (2017), who presented the efficiency of this approach in estimating dynamic factor models defined by latent stochastic processes. Ippoliti et al (2012) used a linear Gaussian state space model to produce predictions of airborne pollutants in Italy and in Mexico.

1.2 Beijing ambient air pollution data

In this paper, we aim at accurately estimating and predicting the concentration of airborne particulate matter using a flexible state space model. We consider a dataset of hourly PM2.5 readings ($\mu\text{g}/\text{m}^3$) and meteorological measurements, such as dew point (DEWP, degrees Celsius), temperature (TEMP, degrees Celsius), pressure (PRES, hPa), wind direction (cbwd, taking values: northwest (NW), northeast (NE), southeast (SE) and calm and variable (CV)), cumulated wind speed (IWS, m/s) and precipitations (PREC), collected in Beijing in 2014, and we split the data into 12 monthly sub-sets¹ (Liang et al (2015)). In order to consider the effects of meteorological conditions on airborne contaminants concentrations, we assume a generalized additive model (GAM) (Hastie and Tibshirani (1986)). More precisely, we suppose that, for each month, the relationship between PM2.5 concentrations Y_t and the meteorological variables \mathbf{x}_t for each hourly data point $t = 1, \dots, T$ (where T is the total number of monthly observations) is described by a GAM, such that

$$Y_t = f(\mathbf{x}_t) + \sigma \varepsilon_t, \quad (5)$$

¹The dataset used in this paper is part of a larger dataset collected in Beijing during a 5-year time period, from January 1st, 2010 to December 31st, 2014, for a total of 43,824 observations. The data are available at <https://archive.ics.uci.edu/ml/datasets/Beijing+PM2.5+Data>

where $f(\cdot)$ is a smooth function of the meteorological covariates, expressing the mean of the GAM, and $\varepsilon_t \stackrel{\text{iid}}{\sim} N(0, \sigma^2)$. We define the variables Z_t as

$$Z_t = \frac{Y_t - f(\mathbf{x}_t)}{\sigma}, \quad (6)$$

for $t = 1, \dots, T$. Using the estimates $\hat{f}(\mathbf{x}_t)$ and $\hat{\sigma}$ of the GAM, we obtain approximately standard normal data \hat{z}_t as

$$\hat{z}_t = \frac{y_t - \hat{f}(\mathbf{x}_t)}{\hat{\sigma}}, \quad (7)$$

for $t = 1, \dots, T$. The empirical autocorrelation function of $(\hat{z}_t)_{t=1, \dots, T}$ is shown for each month in Figure 1. We observe dependence among succeeding observations and therefore the independence assumption for the errors ε_t of the standard GAM model in (5) does not seem to be appropriate.

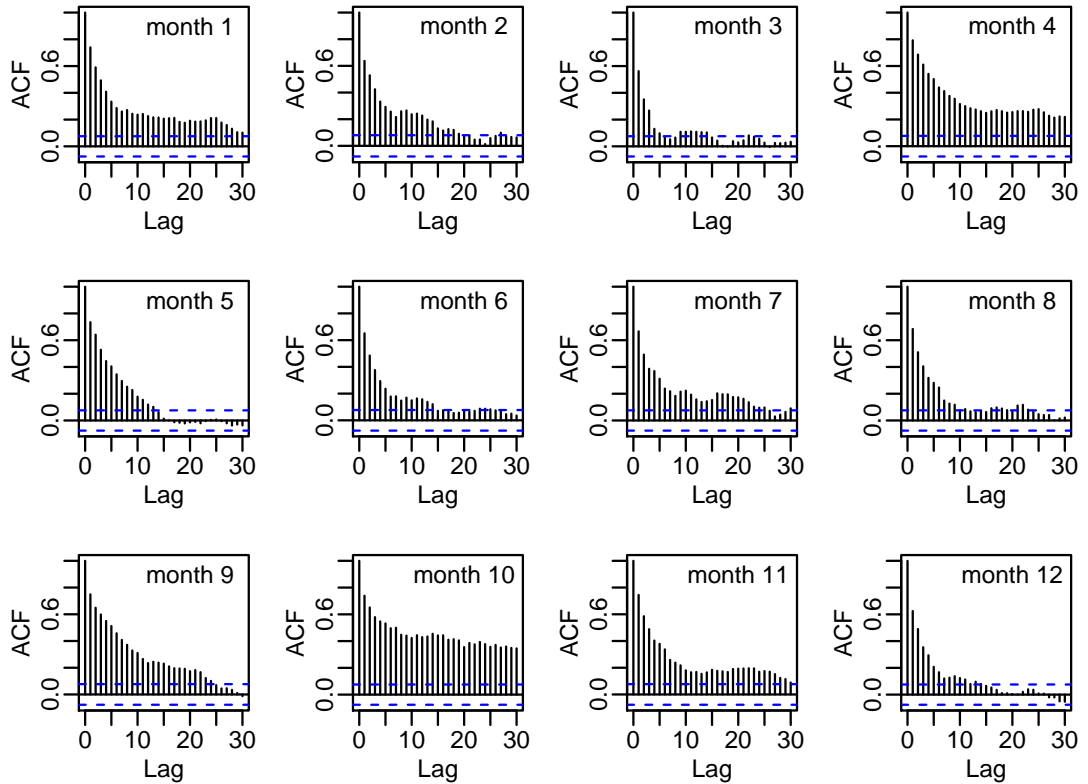


Figure 1: Autocorrelation functions (acf) of $(\hat{z}_t)_{t=1, \dots, T}$ for all 12 training data sets.

We employ a state space model, as specified in (1) and (2), to allow for time effects in the GAM. In our application, ρ_t^{obs} and ρ_t^{lat} will be estimated from the data. Further, we assume that they do not depend on time, i.e. we set $\rho_t^{obs} = \rho^{obs}$ and $\rho_t^{lat} = \rho^{lat}$. We now propose a state space model for Z_t , which is standardized by a GAM. Under our assumptions we have $\sigma_t^{obs} = \sqrt{\text{Var}(Z_t|W_t)} = \sqrt{1 - (\rho^{obs})^2}$ for $\rho^{obs} \in (-1, 1)$ and $\sigma_t^{lat} = \sqrt{\text{Var}(W_t|W_{t-1})} = \sqrt{1 - (\rho^{lat})^2}$ for $\rho^{lat} \in (-1, 1)$. For the initial conditions we assume $\mu_0^{lat} = 0$ and $\sigma_0^{lat} = 1$. With these assumptions the state space model in (1) and (2) becomes

$$\begin{aligned} Z_t &= \rho^{obs} W_t + \sqrt{1 - (\rho^{obs})^2} \eta_t^{obs} \\ W_t &= \rho^{lat} W_{t-1} + \sqrt{1 - (\rho^{lat})^2} \eta_t^{lat} \end{aligned} \quad (8)$$

with $\eta_t^{obs}, \eta_t^{lat} \stackrel{iid}{\sim} N(0, 1)$ and $W_0 \sim N(0, 1)$. Note that representation (8) induces the following bivariate normal distributions

$$\begin{aligned} \begin{pmatrix} Z_t \\ W_t \end{pmatrix} &\sim N_2 \left(\begin{pmatrix} 0 \\ 0 \end{pmatrix}, \begin{pmatrix} 1 & \rho^{obs} \\ \rho^{obs} & 1 \end{pmatrix} \right) \\ \begin{pmatrix} W_t \\ W_{t-1} \end{pmatrix} &\sim N_2 \left(\begin{pmatrix} 0 \\ 0 \end{pmatrix}, \begin{pmatrix} 1 & \rho^{lat} \\ \rho^{lat} & 1 \end{pmatrix} \right). \end{aligned}$$

In order to assess the suitability of the linear Gaussian state space model to the Beijing air pollution data, we display in Figure 2 the bivariate normalized contour plots of the pairs $(\hat{z}_t, \hat{z}_{t-1})_{t=2, \dots, T}$ for each month, to visualize the dependence structure between two successive time points in the series. Using (8) we see that Z_t can be written as a linear function of Z_{t-1} and independent normally distributed disturbances. Since Z_1 is normally distributed, it follows that (Z_t, Z_{t-1}) are jointly normal.

However, Figure 2 reveals that the normalized contour plots of the Beijing monthly data deviate from the elliptical shape of a Gaussian dependence structure (which, to aid comparisons, is depicted in the top left panel of Figure 14 in the Appendix). For example, the contour plot for August (month 8) shows asymmetry in the tails, which cannot be modeled with a Gaussian distribution. This suggests that the linear Gaussian state space model is too restrictive for the Beijing air pollution data and a more flexible approach needs to be adopted.

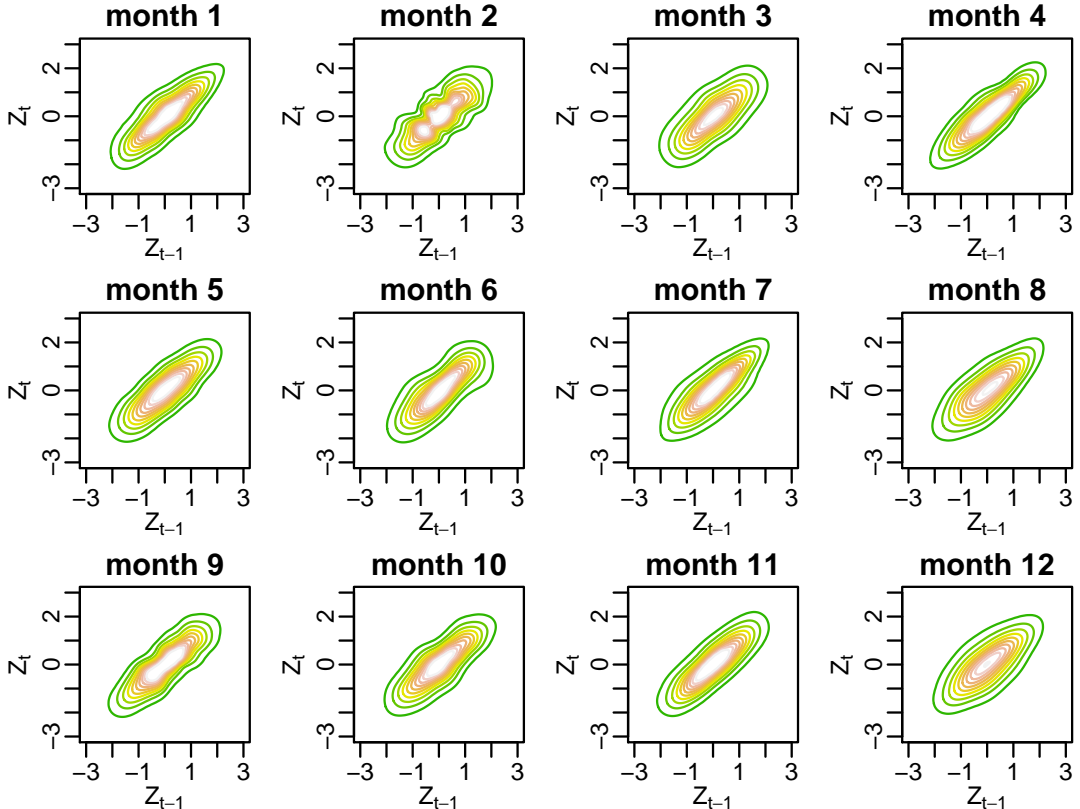


Figure 2: Normalized contour plots of pairs $(\hat{z}_t, \hat{z}_{t-1})_{t=2, \dots, T}$ ignoring serial dependence for each of the 12 Beijing air pollution monthly data sets.

1.3 Our proposal

In the literature, extensions of the linear Gaussian state space model, relaxing the assumptions of linearity and normality, have been studied, for example, by Johns and Shumway (2005), who adopted a non-linear and non-Gaussian state space formulation to model airborne particulate matter, yet relying on the Normal distribution to describe the errors in the state and observation

equations. Chen et al (2012) implemented a non-linear state space model to predict the global burden of infectious diseases using the extended Kalman filter approach. Non-linear state and observation equations of this model were derived from differential equations, however the authors still used Gaussian noise terms in the observation and state equations.

We propose a very flexible Bayesian non-linear and non-Gaussian state space model, where both the observation and the state equations are described by copulas. First, we find an equivalent formulation of the Gaussian state space model in (8) in terms of copulas. The representation is given by

$$\begin{aligned}(U_t, V_t) &\sim \mathbb{C}_{U,V}^{Gauss}(\cdot, \cdot; \tau_{obs}) \\ (V_t, V_{t-1}) &\sim \mathbb{C}_{V_2, V_1}^{Gauss}(\cdot, \cdot; \tau_{lat}),\end{aligned}\tag{9}$$

where

$$U_t = \Phi(Z_t), V_t = \Phi(W_t),\tag{10}$$

with Φ denoting the standard normal cumulative distribution function. The variables U_t and V_t are marginally uniformly distributed on $(0,1)$ and Z_t and W_t are standard normal. Here the Gaussian copulas $\mathbb{C}_{U,V}^{Gauss}$ and $\mathbb{C}_{V_2, V_1}^{Gauss}$ are parametrized by Kendall's τ , obtained as $\tau_{obs} = \frac{2}{\pi} \arcsin(\rho_{obs})$ and $\tau_{lat} = \frac{2}{\pi} \arcsin(\rho_{lat})$. Corresponding approximately uniform pseudo-copula data, that can be used for estimating the model in (9), are obtained as

$$\hat{u}_t = \Phi(\hat{z}_t).\tag{11}$$

By reformulating the state space representation in (8) in terms of copulas in (9), it is straightforward to see how we can generalize the Gaussian linear state space model by replacing the Gaussian copulas in (9) with arbitrary bivariate copulas. Typical restrictions of the Gaussian copula, such as symmetric tails, can be circumvented. For example, a Gumbel copula would allow for asymmetric tails. Koopman et al (2016) incorporated the symmetric-tailed Gaussian and Student t copulas in non-linear non-Gaussian state space models; however, they restricted their attention solely to autoregressive state equations and considered only joint copula densities and not conditional distributions derived from them. The proposed Bayesian copula-based state space model allows us to specify various types of dependence structures to model the relationships between the observations and the underlying states, and to describe the states evolution over time. We will show that our methodology is able to accurately model and predict the levels of PM2.5 in Beijing.

The remainder of the paper is organized as follows. Section 2 introduces a copula-based state space model, Section 3 illustrates the Bayesian inference for the proposed approach, Section 4 is devoted to the application of the copula state space model to the Beijing pollution data. Concluding remarks are given in Section 5.

2 The copula state space model

The copula state space model extends the linear Gaussian state space approach, allowing copula specifications in place of normal distributions as in the observation equation (3) as well as in the state equation (4). In particular, we assume that the dynamic behaviour of the residuals $Z_t := \Phi^{-1}(U_t)$ for the GAM model introduced in equation (5), with $Z_t \sim N(0, 1)$ and $U_t \sim U(0, 1)$ defined as in (10), depends on the latent variable $W_t := \Phi^{-1}(V_t)$, with $W_t \sim N(0, 1)$ and $V_t \sim U(0, 1)$, according to a bivariate copula distribution given in the observation equation. The evolution of the latent variable W_t over time is also described by a bivariate copula distribution, which defines the state equation of the model. The copula distributions defining the observation and state equations of the proposed state space approach do not necessarily belong to the same family, allowing maximum flexibility in the specification of the model. However, we restrict our model to bivariate copula families with a single parameter. This gives still a flexible class of copula families, including e.g. Gaussian, Gumbel, Clayton or Frank copulas. The Student t copula can also be included if we fix the degrees of freedom parameter. An overview of different bivariate copula families can be found in Joe (2014), Chapter 4. Further, we are able to express the copula dependence parameters in the observation and state equations in terms of Kendall's τ . This is convenient for comparison of the dependence strength, since the parameter

space of distinct copula families may be different. More formally, we assume the following joint distributions for the uniformly transformed variables U_t and V_t , with $t = 1, \dots, T$

$$\begin{aligned}(U_t, V_t) &\sim \mathbb{C}_{U,V}^{obs}(\cdot, \cdot; \tau_{obs}) \\ (V_t, V_{t-1}) &\sim \mathbb{C}_{V_2, V_1}^{lat}(\cdot, \cdot; \tau_{lat}),\end{aligned}$$

where $\tau_{obs} = g(\theta_{obs})$ is the Kendall's τ of the copula of the observations and $\tau_{lat} = g(\theta_{lat})$ is the Kendall's τ of the copula of the states (latent variables), respectively. The function g is an appropriate one-to-one transformation function, and θ_{obs} and θ_{lat} are the parameters of the bivariate copulas $\mathbb{C}_{U,V}^{obs}$ and $\mathbb{C}_{V_2, V_1}^{lat}$, respectively. For the specification of g for some one-parameter copula families see Joe (2014), Chapter 4.

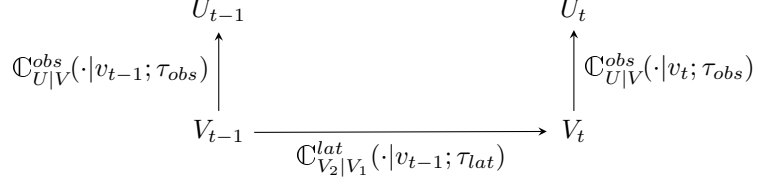


Figure 3: Graphical visualization of the copula state space model.

The copula state space model is defined on the uniform scale as follows

$$U_t | V_t = v_t \sim \mathbb{C}_{U|V}^{obs}(\cdot | v_t; \tau_{obs}) \quad (12)$$

$$V_t | V_{t-1} = v_{t-1} \sim \mathbb{C}_{V_2|V_1}^{lat}(\cdot | v_{t-1}; \tau_{lat}) \quad (13)$$

where (12) is the observation equation and (13) is the state equation. We assume, as in the linear Gaussian state space model, that U_t is independent of U_{t-1} given the latent state V_t . The copula state space model introduced in equations (12) and (13) can be visualized as in Figure 3.

We now derive the joint distributions for the normalized variables Z_t and W_t

$$(Z_t, W_t) \sim F_{Z_t, W_t} \quad (14)$$

$$(W_t, W_{t-1}) \sim F_{W_t, W_{t-1}}. \quad (15)$$

By Sklar's theorem (Sklar (1959)), the distribution (14) can be expressed as

$$\begin{aligned}F_{Z_t, W_t}(z_t, w_t) &= \mathbb{C}_{U,V}^{obs}(\Phi(z_t), \Phi(w_t); \tau_{obs}) \\ &= \mathbb{C}_{U,V}^{obs}(u_t, v_t; \tau_{obs}).\end{aligned}$$

Hence,

$$\begin{aligned}F_{Z_t | W_t = w_t}(z_t | w_t) &= \frac{\partial}{\partial v_t} \mathbb{C}_{U,V}^{obs}(\Phi(z_t), v_t; \tau_{obs}) \Big|_{v_t = \Phi(w_t)} \\ &= \mathbb{C}_{U|V}^{obs}(u_t | v_t; \tau_{obs}) \\ &= \mathbb{C}_{U|V}^{obs}(\Phi(z_t) | \Phi(w_t); \tau_{obs}).\end{aligned}$$

Similarly,

$$F_{W_t | W_{t-1} = w_{t-1}}(\cdot | w_{t-1}) = \mathbb{C}_{V_2|V_1}^{lat}(\Phi(\cdot) | \Phi(w_{t-1}); \tau_{lat}).$$

Therefore, the model can also be expressed on the normalized scale as follows

$$Z_t | W_t = w_t \sim \mathbb{C}_{U|V}^{obs}(\Phi(z_t) | \Phi(w_t); \tau_{obs}) \quad (16)$$

$$W_t | W_{t-1} = w_{t-1} \sim \mathbb{C}_{V_2|V_1}^{lat}(\Phi(w_t) | \Phi(w_{t-1}); \tau_{lat}), \quad (17)$$

where (16) is the observation equation and (17) is the state equation. Contour plots of (Z_t, Z_{t-1}) of this model for different choices of bivariate copulas are shown in Figure 4, illustrating different shapes that the model can deal with.

The copula state space model has the advantage of allowing flexibility in the specification of the observation and state equations, and thus is able to accommodate a wide variety of dependence structures in the air pollution data dynamics. In addition, our methodology allows us to model non-measured autoregressive effects through the underlying latent variable σW_t , as defined on the original scale of the GAM residuals, or via the proxy V_t , on the uniform scale. For our GAM setup we assume that $Y_t \sim N(f(\mathbf{x}_t), \sigma^2)$. Then, the influence of the non-measured autoregressive effect on the response Y_t can be modeled through the conditional distribution of Y_t given $W_t = w_t$. The corresponding conditional expectation is obtained as

$$E(Y_t|W_t = w_t) = f(\mathbf{x}_t) + \sigma E(Z_t|W_t = w_t) = E(Y_t) + \sigma E(Z_t|W_t = w_t).$$

Therefore, $\sigma E(Z_t|W_t = w_t)$ is the difference between the conditional mean $E(Z_t|W_t = w_t)$ and the unconditional mean $E(Y_t)$. We aim at detecting unusual levels of $\sigma E(Z_t|W_t = w_t)$ compared to $f(\mathbf{x}_t)$, to identify time points where conditioning on W_t has a rather big influence on the response. Similarly we can check for unusual levels of the mode or median of $Z_t|W_t = w_t$ compared to $f(\mathbf{x}_t)$.

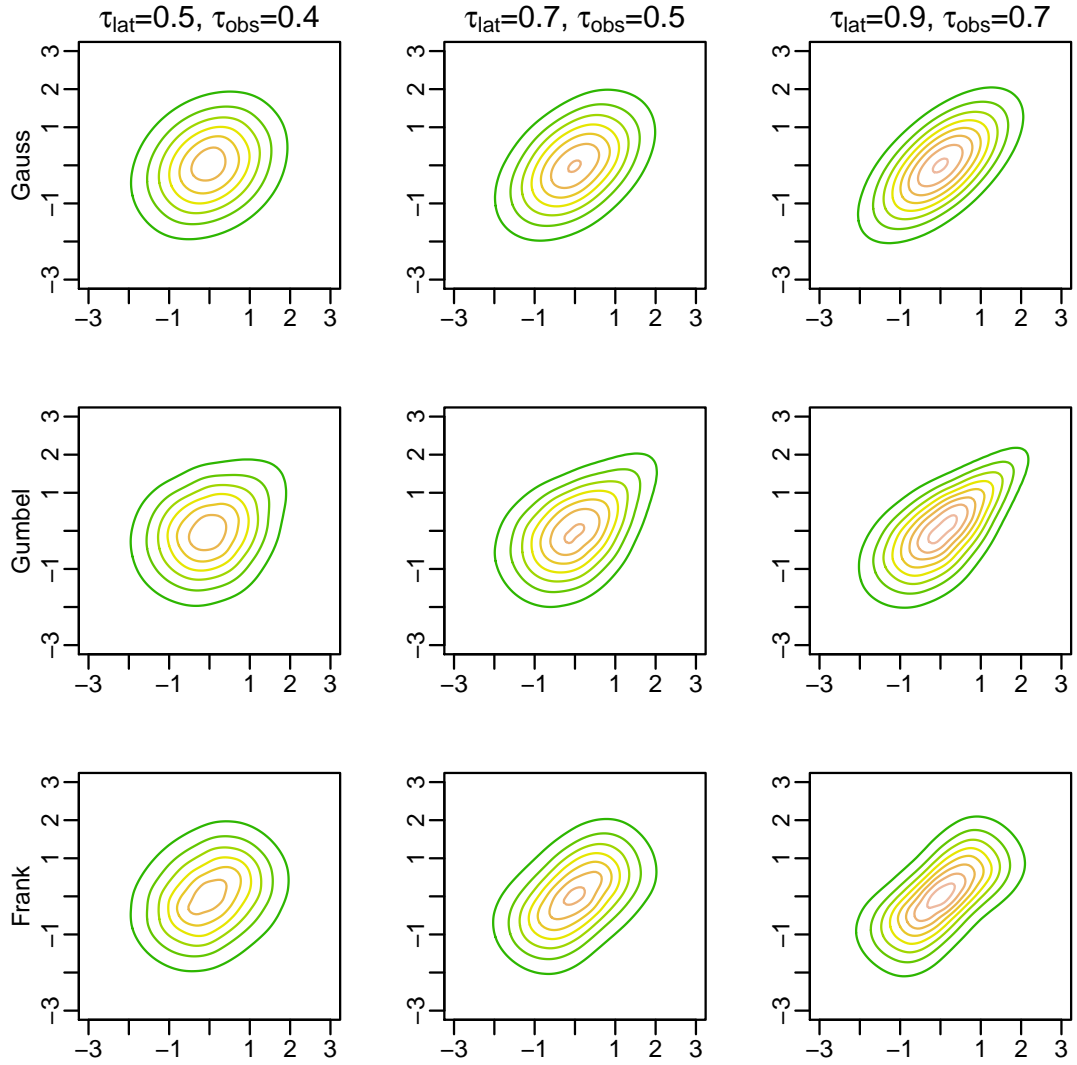


Figure 4: Normalized contour plots for (Z_t, Z_{t-1}) of the copula state space model for different choices of bivariate copula families. In the state and the observation equation we choose the same copula family.

2.1 Identifiability constraints

We notice some identifiability issues related to the model. In particular, if $\tau_{obs} = 1$, then $U_t = V_t$, the observed and latent variables are equivalent and hence the state equation becomes unnecessary. In addition, if $\tau_{lat} = 0$, then the latent variables $(V_t)_{t=1,\dots,T}$ at different time points become independent. Therefore, we need to set identifiability constraints for the copula state space model by establishing a relationship between τ_{obs} and τ_{lat} . In order to do that, we notice that the dependence between two successive time points U_{t-1} and U_t is determined by both τ_{lat} and τ_{obs} . The form of the correlation between $Z_{t-1} = \Phi^{-1}(U_{t-1})$ and $Z_t = \Phi^{-1}(U_t)$ can be derived exactly when $\mathbb{C}_{U,V}^{obs}$ and $\mathbb{C}_{V_2,V_1}^{lat}$ are both Gaussian copulas. Since in the Gaussian case the parameter of the observation equation copula is the correlation coefficient ρ_{obs} and the parameter of the state equation copula is the correlation coefficient ρ_{lat} , then the correlation between Z_{t-1} and Z_t is $\text{cor}(Z_{t-1}, Z_t) = \rho_{obs}^2 \rho_{lat}$. In order to guarantee that the latent states are represented as a smooth curve, we impose that $\rho_{obs} < \rho_{lat}$. In particular, we assume the identifiability constraint in the Gaussian case

$$\rho_{obs} = \rho_{lat}^c \quad \text{for some suitable value} \quad c > 1.$$

In this case, the correlation between Z_{t-1} and Z_t becomes $\text{cor}(Z_{t-1}, Z_t) = \rho_{lat}^{2c+1}$. Transforming the correlation coefficients into Kendall's τ , in the Gaussian case, we obtain the following relationships

$$\tau_{obs} = \frac{2}{\pi} \arcsin(\rho_{lat}^c) \quad \text{and} \quad \tau_{lat} = \frac{2}{\pi} \arcsin(\rho_{obs}),$$

hence, τ_{obs} is a function of τ_{lat} and c .

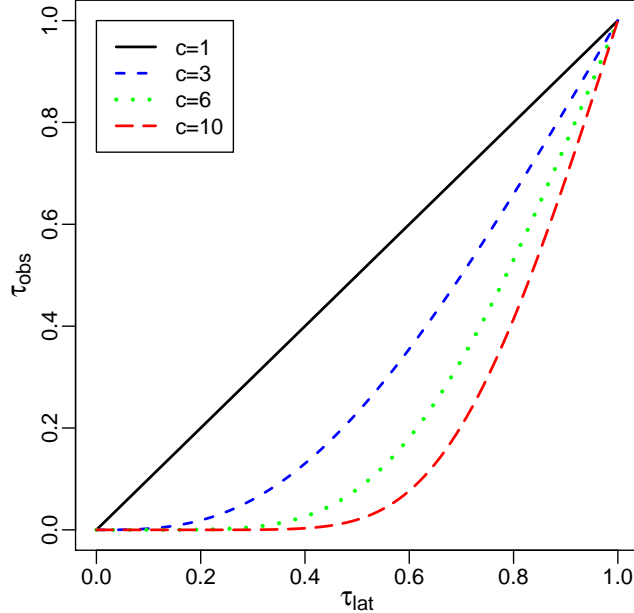


Figure 5: Graphical representation of the relationship between the parameter τ_{obs} (y-axis) plotted against τ_{lat} (x-axis) in the Gaussian case for different values of $c = 1, 3, 6, 10$.

Figure 5 visualizes the relationship between the parameter τ_{obs} (on the y-axis) plotted against τ_{lat} (on the x-axis) in the Gaussian case for different values of $c = 1, 3, 6, 10$. Considering that the strength of dependence between U_{t-1} and U_t is increasing in τ_{lat} and in τ_{obs} , Figure 5 shows that the higher the value of c the higher τ_{lat} needs to be to achieve a fixed strength of dependence between U_{t-1} and U_t . Therefore, for higher values of c we expect to obtain a smoother behaviour of the latent states $(V_t)_{t=1,\dots,T}$. We propose to use a similar relationship between τ_{lat} , τ_{obs} and c , not only in the Gaussian case, but also for arbitrary bivariate copula families. Therefore, in general, we impose the following identifiability constraint on the

copula parameter for all bivariate copula families with a single parameter identified uniquely by Kendall's τ as follows

$$\sin\left(\frac{\pi}{2}\tau_{obs}\right) = \left(\sin\left(\frac{\pi}{2}\tau_{lat}\right)\right)^c \quad \text{for some suitable value } c > 1. \quad (18)$$

3 Bayesian analysis of the copula state space model

3.1 Hamiltonian Monte Carlo

The copula state space model is a highly non-linear and non-Gaussian model, which provides great flexibility by allowing for different bivariate copulas. The downside of this flexibility is that inference for this model is not straight forward, e.g. it is not possible to derive a Gibbs sampler, where we can directly sample from the corresponding full conditionals. For inference for the copula state space model we rely on the No-U-Turn sampler of Hoffman and Gelman (2014) implemented within the STAN framework (Carpenter et al (2016)). The No-U-Turn sampler extends Hamiltonian Monte Carlo (HMC) and adaptively selects tuning parameters. HMC only requires the log posterior density and its derivatives, which are obtained through automatic differentiation (Carpenter et al (2015)) in STAN. The sampler has shown good performance in several other cases (Hajian (2007); Pakman and Paninski (2014); Hartmann and Ehlers (2017)). An alternative Bayesian approach for jointly estimating parameters and states in non-linear non-Gaussian state space models is presented by Barra et al (2017), who designed flexible proposal densities for the independent Metropolis-Hastings and the importance sampling algorithms.

HMC can be considered as a Metropolis Hastings algorithm, where new states are efficiently obtained by using information on the gradient of the log posterior density. Therefore our parameters of interest are interpreted as a position vector $\mathbf{q} \in \mathbb{R}^d$ at time s . Furthermore we assign an associated momentum vector $\mathbf{p} \in \mathbb{R}^d$ at time s . The change of the position vector and the momentum vector over time is described through the function $H(\mathbf{p}, \mathbf{q})$, the *Hamiltonian*, which satisfies the differential equations:

$$\begin{aligned} \frac{dq_i}{ds} &= \frac{dH}{dp_i} \\ \frac{dp_i}{ds} &= -\frac{dH}{dq_i}, \quad i = 1, \dots, d. \end{aligned} \quad (19)$$

Here we assume that $H(\mathbf{q}, \mathbf{p}) = -\pi(\mathbf{q}|D) + \mathbf{p}^t M^{-1} \mathbf{p} / 2$, where $M \in \mathbb{R}^{d \times d}$ is a covariance matrix and $\pi(\mathbf{q}|D)$ is the posterior density for given data D . The Leapfrog method is a popular choice to approximate the solution of the differential equations in (19), which usually cannot be obtained analytically (Neal et al (2011)). For our application, the data are the approximately uniform data $\hat{u}_1, \dots, \hat{u}_T$, obtained as in (11) and the parameter vector \mathbf{q} is given by $\mathbf{q} = (\tau_{lat}, v_1, \dots, v_T)$. Note that for the Bayesian approach the latent variables of the state equation are considered as parameters. The posterior density is obtained as

$$\pi(\mathbf{q}|D) = \prod_{t=1}^T c_{U,V}(\hat{u}_t, v_t; \tau_{obs}) \prod_{t=2}^T c_{V_2, V_1}(v_t, v_{t-1}; \tau_{lat}),$$

where we assume a uniform prior on the interval $(0,1)$ for τ_{lat} as specified in Section 3.2 and τ_{obs} is a function of τ_{lat} as given in (18).

In order to incorporate the function H into a probabilistic framework, a probability distribution can be defined through the canonical distribution. The corresponding canonical density is given by

$$p(\mathbf{q}, \mathbf{p}) := \frac{1}{Z} \exp(-H(\mathbf{p}, \mathbf{q})) = \frac{1}{Z} \pi(\mathbf{q}|D) \exp(-\mathbf{p}^t M^{-1} \mathbf{p} / 2), \quad (20)$$

where \mathbf{q} and \mathbf{p} are independent and Z is a normalizing constant. Hence, the marginal distribution for \mathbf{q} of $p(\mathbf{q}, \mathbf{p})$ in (20) is the desired posterior distribution. Note that the marginal distribution for \mathbf{p} is a multivariate normal distribution with zero mean and covariance matrix M . To sample \mathbf{q} and \mathbf{p} from the canonical distribution specified in (20) we proceed as follows.

1. Sample \mathbf{p} from the normal distribution with zero mean vector and covariance matrix M .
2. Metropolis update: start with the current state (\mathbf{q}, \mathbf{p}) and use the Leapfrog method to simulate L steps of Hamiltonian dynamics with step size ϵ . We obtain a new state $(\mathbf{q}', \mathbf{p}')$ and accept this proposal with Metropolis acceptance probability

$$\min \left(1, \frac{\pi(\mathbf{q}'|D) \exp(\mathbf{p}'^t M^{-1} \mathbf{p}'/2)}{\pi(\mathbf{q}|D) \exp(\mathbf{p}^t M^{-1} \mathbf{p}/2)} \right).$$

In conventional HMC, ϵ , L and M need to be specified by the user. The No-U-Turn sampler sets these tuning parameters adaptively during sampling.

3.2 Posterior inference

As prior distribution for τ_{lat} we use a uniform prior on $(0,1)$, which is a non-informative prior restricted to positive dependence, since we do not expect negative dependence in our application. With this prior specification we obtain a proper Bayesian model and it is straight forward to run the No-U-Turn sampler. For a chosen c we obtain a posterior sample for τ_{lat}

$$\tau_{lat}^r(c), \quad r = 1, \dots, R$$

and, similarly, for τ_{obs} , using the relationship in (18),

$$\tau_{obs}^r(c), \quad r = 1, \dots, R$$

where R is the total number of HMC iterations. Additionally, posterior samples for the latent variables V_t , for $t = 1, \dots, T$, are denoted by

$$v_t^r(c), \quad t = 1, \dots, T \quad \text{and} \quad r = 1, \dots, R.$$

3.3 Predictive simulation

An advantage of the Bayesian approach is that our model already specifies the predictive distribution, which is the distribution of the response one or several days ahead. From this distribution uncertainty is easy to be quantified through credible intervals.

We consider a posterior sample of the model parameters given by the set $\{\tau_{lat}^r(c), v_t^r(c), r = 1, \dots, R, t = 1, \dots, T\}$. Then, simulated values from the one-day-ahead predictive distribution of V_{T+1} given V_T and U_{T+1} given U_T , respectively, can be obtained as follows

- simulate $v_{T+1}^r(c)$ from $\mathbb{C}_{V_2|V_1}^{lat}(\cdot | v_T^r(c), g^{-1}(\tau_{lat}^r(c)))$,
- simulate $u_{T+1}^r(c)$ from $\mathbb{C}_{U|V}^{obs}(\cdot | v_{T+1}^r(c), g^{-1}(\tau_{obs}^r(c)))$.

This gives us a posterior predictive sample $\{u_{T+1}^r(c), r = 1, \dots, R\}$ on the copula scale. We define now

$$\hat{\varepsilon}_{T+1}^r(c) := \Phi^{-1}(u_{T+1}^r(c))$$

as posterior predictive standardized residuals of the GAM model specified in (5). In particular we estimate $E(Y_t)$ by $\hat{f}(\mathbf{x}_t)$ with estimated error variance $\hat{\sigma}^2$. So,

$$\hat{y}_{T+1}^r(c) := \hat{f}(\mathbf{x}_{T+1}) + \hat{\sigma} \hat{\varepsilon}_{T+1}^r(c)$$

gives a posterior sample value of the predicted one-day-ahead response. Therefore, we have a one-day-ahead predictive sample of the response, given by $\{\hat{y}_{T+1}^r(c), r = 1, \dots, R\}$. Note that to obtain this predictive sample we ignore the uncertainty in the marginal distribution.

In general, the prediction value of the response i days ahead, $\hat{y}_{T+i}^r(c)$, can be obtained recursively through:

- simulate $v_{T+i}^r(c) \sim \mathbb{C}_{V_2|V_1}^{lat}(\cdot | v_{T+i-1}^r(c), g^{-1}(\tau_{lat}^r(c)))$,
- simulate $u_{T+i}^r(c) \sim \mathbb{C}_{U|V}^{obs}(\cdot | v_{T+i}^r(c), g^{-1}(\tau_{obs}^r(c)))$,
- define $\hat{\varepsilon}_{T+i}^r(c) := \Phi^{-1}(u_{T+i}^r(c))$,
- set $\hat{y}_{T+i}^r(c) := \hat{f}(\mathbf{x}_{T+i}) + \hat{\sigma}\hat{\varepsilon}_{T+i}^r(c)$.

4 Data analysis

Recall the hourly data set discussed in Section 1.2 divided into 12 sub data sets, one data set for each month. Each of these 12 data sets is further split into training and test data, where the training data consists of the first 90% of the observations and the test data of the remaining 10%. So approximately the first 27 days of the month are used for training and the remaining three days for testing the model.

4.1 Marginal models

For each of the 12 training data sets we fit a GAM using the R package `mgcv` of Wood and Wood (2015), where the response is the logarithm of PM2.5 and the covariates are DEWP, TEMP, PRES, IWS, PREC and cbwd, as described in Section 1.2. We define one additional covariate PREC.ind, which indicates if there is precipitation, i.e. $PREC.ind = \mathbb{1}_{PREC>0}$. Liang et al (2015) showed that the wind direction not only has influence on the response itself, but might also influence the relationship between other covariates and the response. Therefore we allow for different smooth terms corresponding to different wind directions. More precisely, we create four indicator variables corresponding to the four wind directions $\mathbb{1}_{cbwd=CV}$, $\mathbb{1}_{cbwd=NE}$, $\mathbb{1}_{cbwd=NW}$ and $\mathbb{1}_{cbwd=SE}$. Then we replicate the part of the model matrix corresponding to a covariate x four times and multiply each of the four parts with one of the indicator variables $\mathbb{1}_{cbwd=CV}$, $\mathbb{1}_{cbwd=NE}$, $\mathbb{1}_{cbwd=NW}$ and $\mathbb{1}_{cbwd=SE}$. So we obtain four smooth terms corresponding to the covariate x . We do not allow for these interactions with the covariate PREC since this variable has only few values not equal to zero. For variable selection the approach of Marra and Wood (2011) is used, which allows terms to be penalized to zero.

Plots of the different estimated smooth components are shown in Figure 6 for the November (month 11) data set. Plots of the estimated smooth terms in Figure 6 indicate that the covariates have an effect on PM2.5. For example, with northwestern winds (NW), PM2.5 is lower for higher temperatures (TEMP). Furthermore, we draw the same conclusion as Liang et al (2015), that different smooth terms are necessary for different wind directions. For example, with northwestern winds (NW), we do not see influence of the covariate PRES on PM2.5, whereas with southeastern winds (SE), PM2.5 decreases as PRES increases.

4.2 Model selection of monthly copula family and value of c based on average out-of-sample CRPS

We now consider model selection for the copula state space model. This includes the selection of the copula families and the selection of the value of c . We fit models with different copula families and different values of c and select the model which produces the best forecasts. The accuracy of forecasts is evaluated with the continuous ranked probability score (CRPS) (Gneiting and Raftery (2007)).

We have one GAM specification for each month and obtain, for each month, approximately Uniform(0,1) pseudo-copula data \hat{u}_t by the probability integral transform $\hat{u}_t = \Phi\left(\frac{y_t - \hat{f}(\mathbf{x}_t)}{\hat{\sigma}}\right)$ for $t = 1, \dots, T$ as in (11). Here \hat{f} and $\hat{\sigma}$ are the estimates of the GAM and T denotes the number of observation in the training data set of the corresponding month. To simplify notation we avoid indexing the models by month.

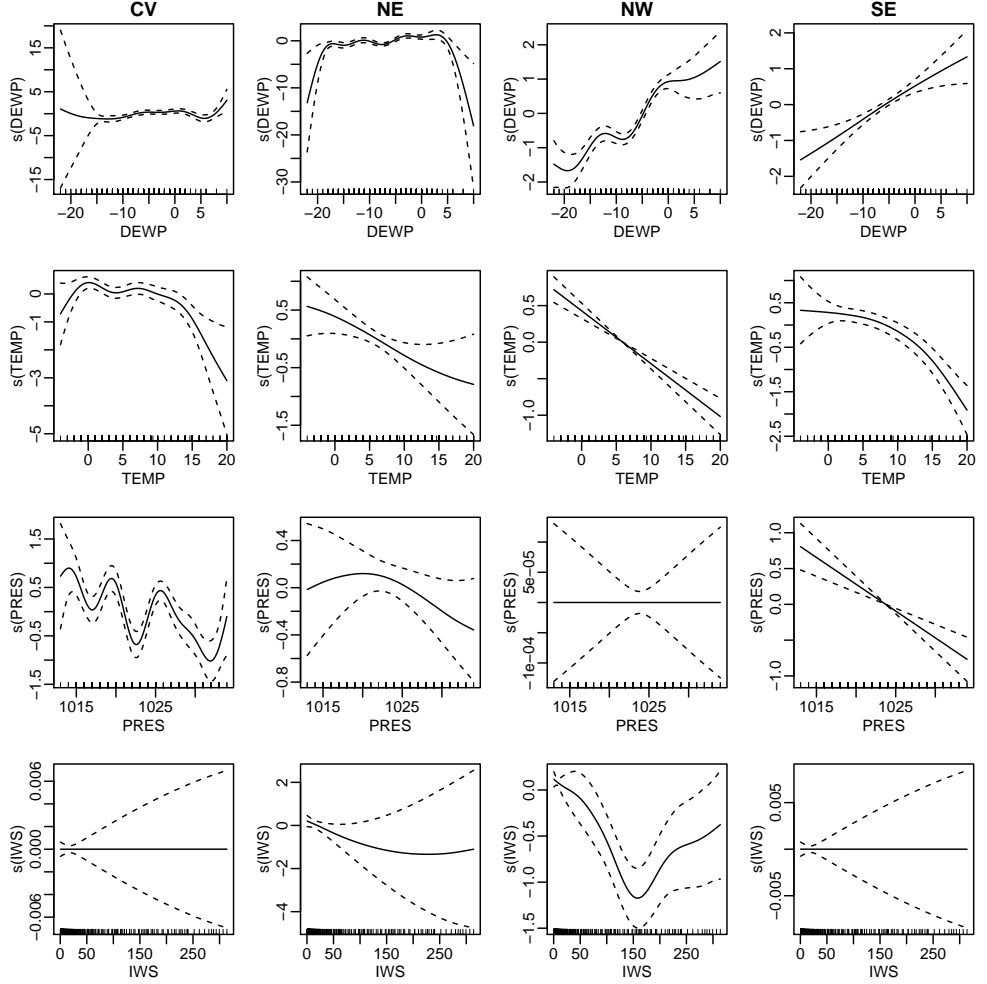


Figure 6: Estimated smooth components of the GAM for month 11 for the continuous covariates DEWP, TEMP, PRES and IWS. For each covariate we have four different smooth terms corresponding to the four wind directions: CV, NE, NW, and SE. The dashed lines represent a pointwise 95% confidence band.

In the following we study several models that can be divided into three model classes.

- **Gaussian state space model \mathcal{M}_{Gauss}** : $\mathbb{C}_{U,V}^{obs}$ and $\mathbb{C}_{V_2,V_1}^{lat}$ are both Gaussian copulas.
- **Copula based state space model \mathcal{M}_{Cop}** : $\mathbb{C}_{U,V}^{obs}$ and $\mathbb{C}_{V_2,V_1}^{lat}$ are from the same bivariate copula family.
- **GAM model with independent errors \mathcal{M}_{Ind}** : $\mathbb{C}_{U,V}^{obs}$ and $\mathbb{C}_{V_2,V_1}^{lat}$ are both independence copulas. This corresponds to a standard GAM model with independent errors.

For each of the 12 training data sets on the copula scale, corresponding to each month of the year, the three model classes are fitted. To estimate model parameters we run the No-U-Turn sampler with 2 chains, where each chain contains 2000 iterations. The first 500 iterations are discarded for burnin. Preliminary analysis showed that this burnin choice is sufficient. We fit the independence model \mathcal{M}_{Ind} , the Gaussian model \mathcal{M}_{Gauss} for every value of $c = 1, 3, 6, 10$ and several latent copula models for the class \mathcal{M}_{Cop} . The different state space copula models correspond to all combinations of the values of $c = 1, 3, 6, 10$ and of a subset of the following bivariate parametric copula families: Student t (df=4), Student t (df=6), Gumbel, Clayton and Frank. This set includes copula families that are appropriate for the observed contour plots in Figure 2 and are shown in Table 1. For example we use, among others, a Gumbel copula for August or a Frank copula for November. So for one specific monthly data set a model is specified by the value of c and the copula family.

Table 1: Allowed copula families for the different monthly data sets. The bivariate Student t copula with ν degrees of freedom is denoted by $t(\nu)$.

month	family
1	$t(6)$, Gumbel
2	$t(4)$, $t(6)$, Frank
3	$t(6)$, Frank
4	$t(4)$, $t(6)$, Gumbel
5	$t(6)$, Frank
6	$t(6)$, Frank
7	$t(6)$, Gumbel
8	$t(4)$, $t(6)$, Gumbel
9	$t(6)$, Frank
10	$t(6)$, Gumbel
11	Frank
12	$t(4)$, $t(6)$, Gumbel

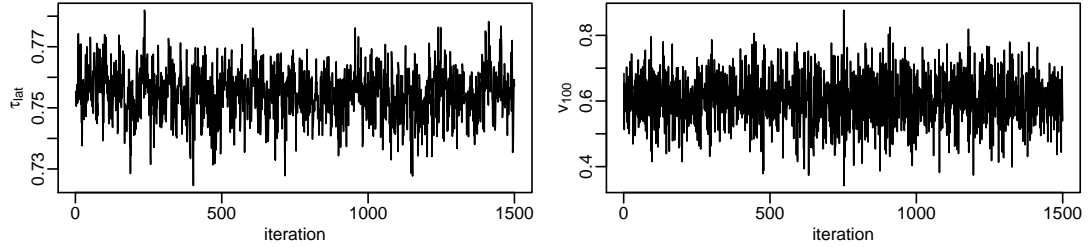


Figure 7: Traceplots of 1500 posterior draws after a burnin of 500 iterations of τ_{lat} (left) and V_{100} (right) of the first chain of the HMC sampler for the model with Frank copulas and $c = 6$ using the training data set for November.

As an example we have a closer look at the model for November with Frank copulas and $c = 6$. Figure 7 shows the traceplots of the dependence parameter τ_{lat} and the latent state at time point 100 (V_{100}) for the first chain. The traceplots suggest that the chains have converged. The chain for τ_{lat} converges to values far away from zero, thus showing dependence. Figure 8 illustrates the effect of the different values of c on the posterior mode estimates of the latent states \hat{v}_t . We observe that oscillations decrease as the value of c increases. However the difference seems not to be very high.

We predict now the response values of the 12 test data sets as described in Section 3.3. The test data sets contain approximately 72 data points, which correspond to every hour in a three days period. For illustration we use the model for November with Frank copulas and $c = 6$ as above. Figure 9 shows predictive densities for different time steps ahead for this model, more precisely the estimated forecast density of Y_{T+t} for $t = 1, 12, 24, 48$ hours based on 3000 HMC iterations from two chains. As we see from this figure, we obtain non-Gaussian forecast densities. Further, the densities are more disperse for a longer time period ahead, reflecting the fact that uncertainty increases if we predict a longer time period ahead. Figure 10 shows how the out-of-sample estimated posterior mode of the latent state on the normal scale \hat{w}_{T+t} and its 90% credible interval evolve over time. For estimating the bounds of the credible intervals, the parameters of the GAM are fixed. We see that the posterior mode moves to zero and the credible interval gets wider as time evolves. This shows how the effect of the latent state at time T on the latent state at time $T + t$ decreases as t increases.

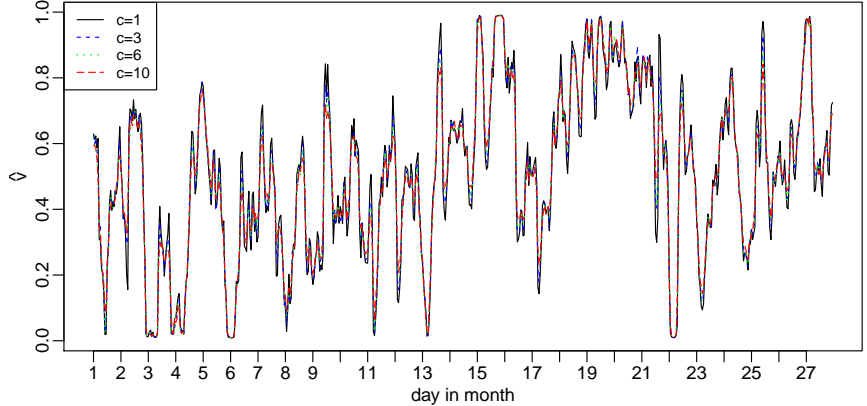


Figure 8: Estimated hourly posterior mode of the latent state \hat{v}_t at time t plotted against t ($t = 1, \dots, T$) for models with Frank copulas and different values of c ($c = 1, 3, 6, 10$) using the training data set for November. The posterior mode estimates are based on 3000 iterations from two chains.

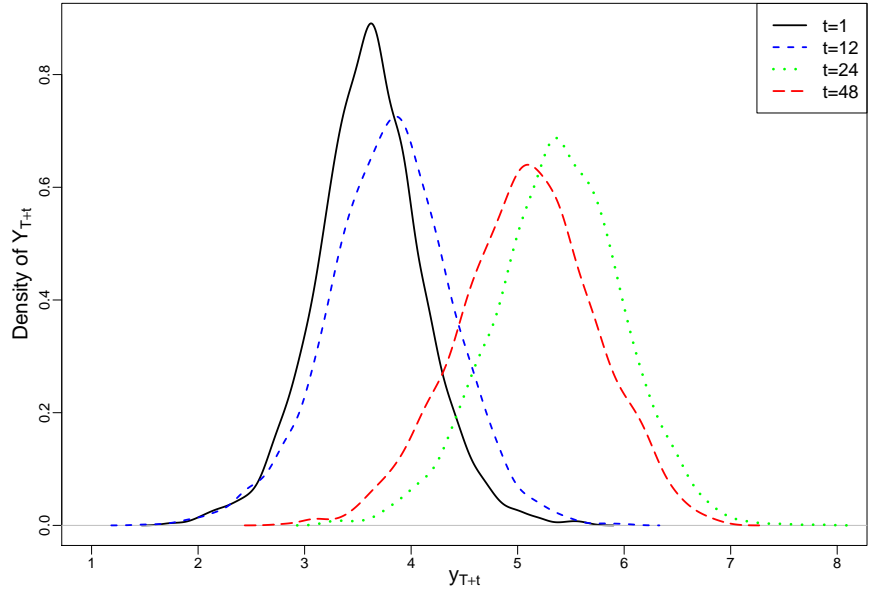


Figure 9: Estimated predictive density of Y_{T+t} from a copula state space model for November with Frank copulas and $c = 6$ for different time steps (hours) ahead ($t = 1, 12, 24, 48$).

For every model characterized by c and the copula family, we calculate the CRPS for every data point in the test set and average over the CRPS per model over every data point. Models are selected with respect to the lowest average CRPS. Table 2 shows the best model in \mathcal{M}_{Cop} , characterized by the value of c and the copula family, and the best model in \mathcal{M}_{Gauss} , characterized by the value of c . In addition Table 2 shows the average CRPS of the best model within the model classes \mathcal{M}_{Cop} , \mathcal{M}_{Gauss} and \mathcal{M}_{Ind} . For August (month 8), the best model is provided by a Gumbel copula. For this month we have already noticed asymmetry in the tails in the corresponding normalized contour plot in Figure 2, which is a feature that can be modeled with a Gumbel copula, but not with a Gaussian one. Further, we see that in 7 out of 12 cases, the best model according to the average CRPS is provided by the copula based model class \mathcal{M}_{Cop} . Furthermore, in cases where the best model is not provided by \mathcal{M}_{Cop} , the difference in average CRPS between the best model in \mathcal{M}_{Cop} and the overall best model is rather small.

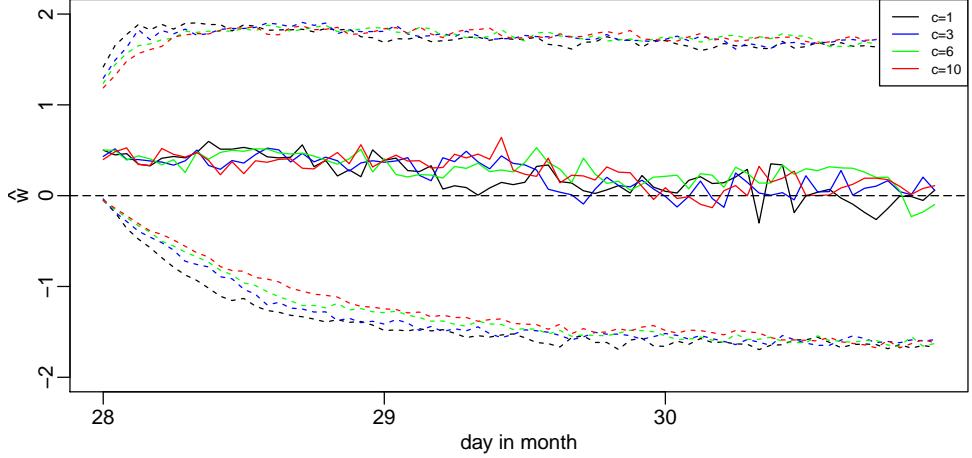


Figure 10: Estimated posterior mode of the latent state on the normal scale at t time steps ahead \hat{w}_{T+t} plotted against $T+t$ for the model for November with Frank copulas and different values of c ($c = 1, 3, 6, 10$). The 5% quantile and 95% quantile are used to construct a 90% credible interval (dashed lines).

Table 2: Family of the best model in \mathcal{M}_{Cop} , value of c of the best model in \mathcal{M}_{Cop} and the best model in \mathcal{M}_{Gauss} and the average CRPS of the best model within each class \mathcal{M}_{Cop} , \mathcal{M}_{Gauss} and \mathcal{M}_{Ind} . The best model is selected with respect to the average CRPS.

month	\mathcal{M}_{Cop}	family		\mathcal{M}_{Cop}	\mathcal{M}_{Gauss}	CRPS		
		\mathcal{M}_{Cop}	c			\mathcal{M}_{Cop}	\mathcal{M}_{Gauss}	\mathcal{M}_{Ind}
1	Gumbel	3	10	0.474	0.479	0.490		
2	$t(6)$	1	1	0.952	0.957	0.949		
3	Frank	6	10	1.109	1.134	1.168		
4	Gumbel	10	10	0.251	0.261	0.253		
5	Frank	1	1	0.328	0.327	0.328		
6	Frank	10	6	0.259	0.257	0.257		
7	$t(6)$	6	10	0.266	0.266	0.276		
8	Gumbel	10	10	0.339	0.354	0.350		
9	$t(6)$	1	1	0.354	0.355	0.356		
10	$t(6)$	10	10	0.455	0.452	0.445		
11	Frank	10	3	0.400	0.410	0.433		
12	Gumbel	10	10	0.605	0.616	0.620		

4.3 Inference for 2014 (in-sample)

In the previous section we selected the best copula state space models according to the lowest average CRPS over the test data. This gave the copula family choice and the value of c for \mathcal{M}_{Cop} and the value of c for \mathcal{M}_{Gauss} . For these choices the complete data of 2014 was refitted for each model class \mathcal{M}_{Ind} , \mathcal{M}_{Gauss} and \mathcal{M}_{Cop} . Further the GAM models in (5) are used for the margins. Figure 11 shows the estimated posterior densities for the dependence parameter τ_{lat} for these models. We observe that most of the mass of the posterior density concentrates between 0.7 and 0.9 for all monthly models. This range for τ_{lat} coincides with positive dependence between two succeeding time points. We also see differences between \mathcal{M}_{Cop} and \mathcal{M}_{Gauss} for some months.

As explained in Section 2, we are interested in the distribution of Z_t conditioned on the latent state W_t . Therefore we simulate from Z_t conditional on $V_t = \hat{v}_t$, where \hat{v}_t is the posterior mode estimate of V_t . In Figure 12 we see the mode of this distribution together with a credible region for the best model in the \mathcal{M}_{Gauss} class and the best model in the \mathcal{M}_{Cop} class for the data in January and November. In addition we adjust $Z_t|V_t = \hat{v}_t$ by the estimated mean $\hat{f}(\mathbf{x}_t)$ and the estimated standard deviation $\hat{\sigma}$ of the GAM to investigate the influence of conditioning

on the latent state on the response (see Section 2). Figure 13 shows the mode and credible regions for $\hat{\sigma} Z_t / \hat{f}(\mathbf{x}_t)$ conditional on $V_t = \hat{v}_t$, with $\hat{\sigma}$, \hat{f} fixed, for the same data and models.

In January, the best model in \mathcal{M}_{Cop} is based on Gumbel copulas. We see from Figure 12 that this model allows for credible regions which are asymmetric around the mode. Asymmetric credible regions cannot be obtained from a Gaussian model.

Further we see from Figures 12 and 13 that on January 18th, the mode is high. On this day unusual high pollution was recorded in Beijing². The copula based state space model with a Gumbel copula has a higher peak on that day compared to the Gaussian state space model. We conclude that the copula based state space model is able to capture this unusual behaviour more appropriately than the Gaussian model.

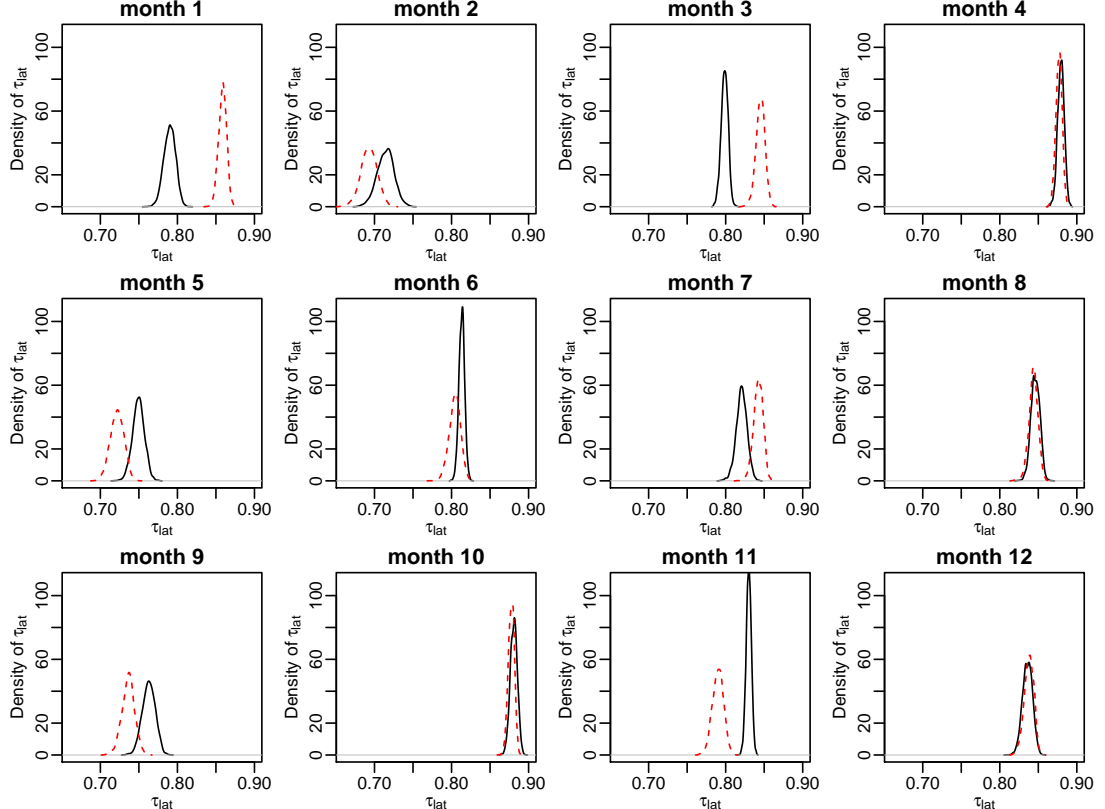


Figure 11: Estimated posterior density of the dependence parameter τ_{lat} for the best model in \mathcal{M}_{Cop} (black) and \mathcal{M}_{Gauss} (red, dashed) according to the average CRPS for all 12 data sets.

5 Summary and Outlook

The starting point of this paper was the question of how to capture not only non-linear effects of meterological variables on pollution measures such as airborne particulate matter, but also to allow for further time dynamics of the observations not covered by the meterological variables. For this we investigated hourly data on ambient air pollution in Beijing and illustrated that the lag-one time dynamics is not a Gaussian one, thus ruling out standard linear state space models.

To deal with this non-Gaussian dependence we proposed a novel non-linear state space model based on a copula formulation for univariate observation and state equations. The observation and state variables are coupled using two bivariate copulas. Since the copula approach allows for separate modeling of the margins and dependence, the observation variables are allowed to follow any time invariant statistical model.

²See <http://www.takepart.com/article/2014/01/18/beijing-china-air-pollution-billboard>

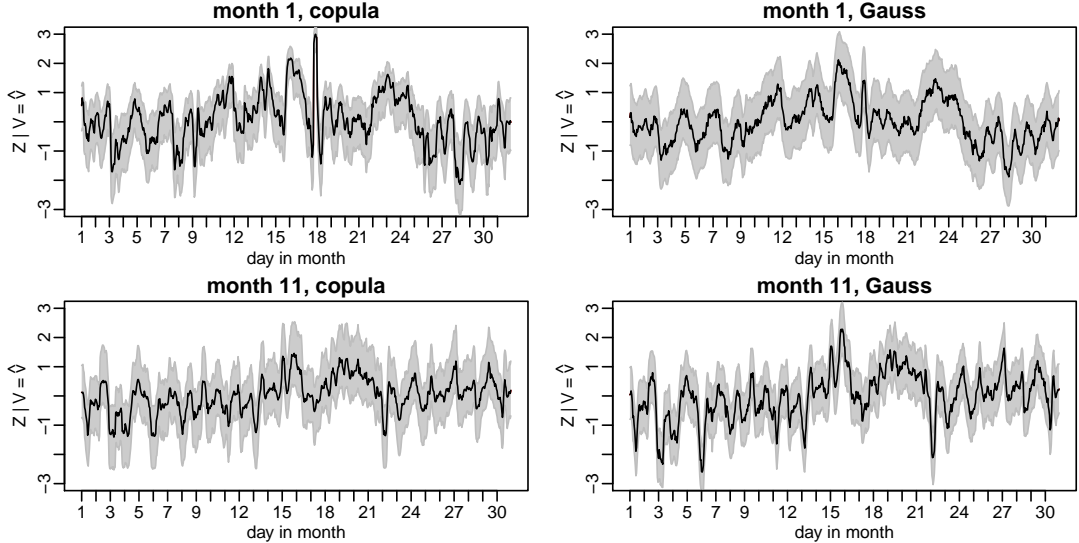


Figure 12: Estimated mode of $Z_t|V_t = \hat{v}_t$, where \hat{v}_t is the posterior mode estimate of V_t , plotted against t for every data point in January and November for the best model in \mathcal{M}_{Cop} (left) and in \mathcal{M}_{Gauss} (right). A 90% credible region, constructed from the 5% and 95% quantile, is added in grey.

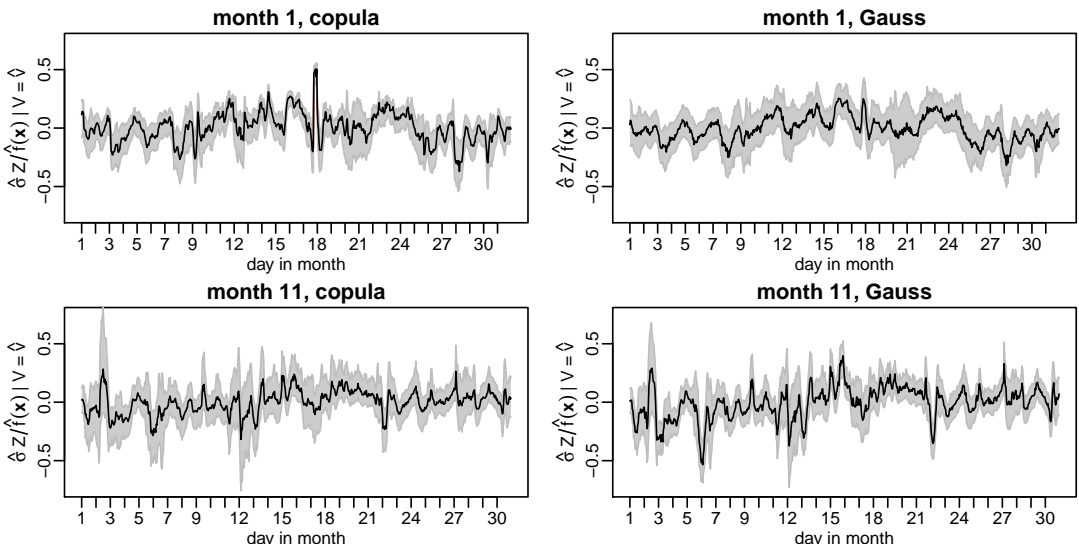


Figure 13: Estimated mode of $\hat{\sigma} Z_t/\hat{f}(x_t)|V_t = \hat{v}_t$, where \hat{v}_t is the posterior mode estimate of V_t , plotted against t for every data point in January and November for the best model in \mathcal{M}_{Cop} (left) and in \mathcal{M}_{Gauss} (right). A 90% credible region, constructed from the 5% and 95% quantile, is added in grey.

In the application we utilized a GAM to allow for non-linear effects of covariates. Once the marginal distribution of the response variables is specified, they can be transformed to the uniform scale using the probability integral transform (PIT). The resulting PIT value at time t is then coupled with $[0,1]$ valued state variables for time t using a bivariate copula. Therefore, the observation equation of the copula based state space formulation is given by the conditional distribution of the PIT value at t given the value of the state variable at time t . The time dynamics of the state variables is then similarly modeled as the conditional distribution of the state variable at time t given the state variable at time $t-1$, where these two state variables are jointly modeled by a bivariate copula. We first show that, in the case of bivariate Gaussian copula, standard linear state space models result. Since many different parametric

bivariate copulas exist, the flexibility of the copula-based state space model is evident and thus a significant extension of linear Gaussian state space models is possible.

Of course, such an extension has its price. In our case this means we cannot follow a standard estimation approach as provided by the Kalman filter approach for linear state space models. Therefore we propose and develop a Bayesian approach based on HMC. Further we deal with some identifiability issues of the copula state space, which we solve by restricting the strength of the dependence among the lag-one state space variables to be higher than the one of the PIT observations and the state variable at time t . This is a natural assumption, since the dynamics of the latent state variable should be less variable than the one arising from the observation and state variable.

The state variables can be interpreted as a way to capture non-measured effects and thus are very appropriate for the data set analyzed in this paper. It allowed us to identify unusual high levels of pollution, which were not captured by the measured variables, in a better way than a copula state space model with Gaussian copulas. We also present, with appropriate normalized bivariate contour plots, explorative tools to detect non-Gaussian dependence structures between lagged PIT transformed observations.

The approach first proposed here allows a wide range of extensions, such as adding covariates for the dependence parameter of the bivariate copulas as well as extending to multivariate response data with a single set of state variables or separate sets of state variables. Here the use of vine copulas can be envisioned wherever higher-dimensional than bivariate copulas are needed. Another route of extension would be to model the bivariate copulas completely nonparameteric. In this case the identifiability issues have to be reworked.

Acknowledgements

The second author was supported by a Global Challenges for Women in Math Science Entrepreneurial Programme grant for a project entitled “Bayesian Analysis of State Space Factor Copula Models” provided by the Technical University of Munich. The third author is supported by the German Research Foundation (DFG grant CZ 86/4-1). Computations were performed on a Linux cluster supported by DFG grant INST 95/919-1 FUGG.

Appendix: Contour plots of bivariate copula densities

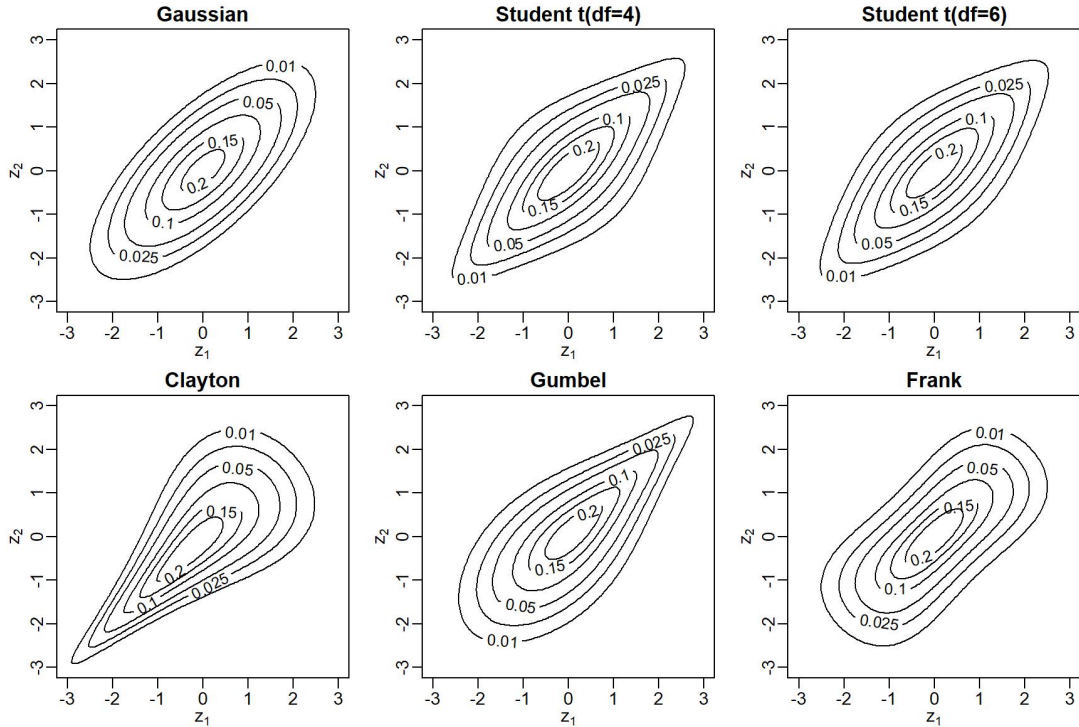


Figure 14: Normalized contour plots of bivariate copula families with Kendall's $\tau = 0.5$.

References

Barra I, Hoogerheide L, Koopman SJ, Lucas A (2017) Joint Bayesian Analysis of Parameters and States in Nonlinear non-Gaussian State Space Models. *Journal of Applied Econometrics* 32(5):1003–1026

Van den Brakel J, Roels J (2010) Intervention analysis with state-space models to estimate discontinuities due to a survey redesign. *The Annals of Applied Statistics* pp 1105–1138

Carpenter B, Hoffman MD, Brubaker M, Lee D, Li P, Betancourt M (2015) The stan math library: Reverse-mode automatic differentiation in C++. arXiv preprint arXiv:150907164

Carpenter B, Gelman A, Hoffman M, Lee D, Goodrich B, Betancourt M, Brubaker MA, Guo J, Li P, Riddell A (2016) Stan: A probabilistic programming language. *Journal of Statistical Software* 20

Chen S, Fricks J, Ferrari MJ (2012) Tracking measles infection through non-linear state space models. *Journal of the Royal Statistical Society: Series C (Applied Statistics)* 61(1):117–134

Cohen AJ, Brauer M, Burnett R, Anderson HR, Frostad J, Estep K, Balakrishnan K, Brunekreef B, Dandona L, Dandona R, et al (2017) Estimates and 25-year trends of the global burden of disease attributable to ambient air pollution: an analysis of data from the Global Burden of Diseases Study 2015. *The Lancet* 389(10082):1907–1918

Dominici F, McDermott A, Zeger SL, Samet JM (2002) On the use of generalized additive models in time-series studies of air pollution and health. *American journal of epidemiology* 156(3):193–203

Durbin J, Koopman SJ (2000) Time series analysis of non-Gaussian observations based on state space models from both classical and Bayesian perspectives. *Journal of the Royal Statistical Society: Series B (Statistical Methodology)* 62(1):3–56

Durbin J, Koopman SJ (2002) A simple and efficient simulation smoother for state space time series analysis. *Biometrika* 89(3):603–616

Durbin J, Koopman SJ (2012) Time series analysis by state space methods, vol 38. Oxford University Press

Gneiting T, Raftery AE (2007) Strictly proper scoring rules, prediction, and estimation. *Journal of the American Statistical Association* 102(477):359–378

Guo Y, Zeng H, Zheng R, Li S, Barnett AG, Zhang S, Zou X, Huxley R, Chen W, Williams G (2016) The association between lung cancer incidence and ambient air pollution in China: a spatiotemporal analysis. *Environmental research* 144:60–65

Hajian A (2007) Efficient cosmological parameter estimation with Hamiltonian Monte Carlo technique. *Physical Review D* 75(8):083,525

Hao H, Chang HH, Holmes HA, Mulholland JA, Klein M, Darrow LA, Strickland MJ (2015) Air pollution and preterm birth in the US State of Georgia (2002–2006): associations with concentrations of 11 ambient air pollutants estimated by combining Community Multiscale Air Quality Model (CMAQ) simulations with stationary monitor measurements. *Environmental health perspectives* 124(6):875–880

Hartmann M, Ehlers RS (2017) Bayesian inference for generalized extreme value distributions via Hamiltonian Monte Carlo. *Communications in Statistics-Simulation and Computation* pp 1–18

Hastie T, Tibshirani R (1986) Generalized Additive Models. *Statistical Science* 1(3):297–318

Hoffman MD, Gelman A (2014) The No-U-turn sampler: adaptively setting path lengths in Hamiltonian Monte Carlo. *Journal of Machine Learning Research* 15(1):1593–1623

Ippoliti L, Valentini P, Gamerman D (2012) Space–time modelling of coupled spatiotemporal environmental variables. *Journal of the Royal Statistical Society: Series C (Applied Statistics)* 61(2):175–200

Joe H (2014) Dependence modeling with copulas. Chapman and Hall/CRC

Johns CJ, Shumway RH (2005) A non-linear and non-Gaussian state-space model for censored air pollution data. *Environmetrics: The official journal of the International Environmetrics Society* 16(2):167–180

Koopman SJ, Mesters G (2017) Empirical Bayes Methods for Dynamic Factor Models. *Review of Economics and Statistics* 99(3):486–498

Koopman SJ, Lucas A, Scharth M (2016) Predicting time-varying parameters with parameter-driven and observation-driven models. *Review of Economics and Statistics* 98(1):97–110

Liang X, Zou T, Guo B, Li S, Zhang H, Zhang S, Huang H, Chen SX (2015) Assessing Beijing’s PM2. 5 pollution: severity, weather impact, APEC and winter heating. *Proc R Soc A* 471(2182):20150,257

Liu M, Huang Y, Ma Z, Jin Z, Liu X, Wang H, Liu Y, Wang J, Jantunen M, Bi J, et al (2017) Spatial and temporal trends in the mortality burden of air pollution in China: 2004–2012. *Environment international* 98:75–81

Marra G, Wood SN (2011) Practical variable selection for generalized additive models. *Computational Statistics & Data Analysis* 55(7):2372–2387

Neal RM, et al (2011) MCMC using Hamiltonian dynamics. *Handbook of Markov Chain Monte Carlo* 2:113–162

Pakman A, Paninski L (2014) Exact hamiltonian monte carlo for truncated multivariate gaussians. *Journal of Computational and Graphical Statistics* 23(2):518–542

Sahu SK, Gelfand AE, Holland DM (2006) Spatio-temporal modeling of fine particulate matter. *Journal of Agricultural, Biological, and Environmental Statistics* 11(1):61

Shaddick G, Thomas ML, Green A, Brauer M, van Donkelaar A, Burnett R, Chang HH, Cohen A, Van Dingenen R, Dora C, et al (2018) Data integration model for air quality: a hierarchical approach to the global estimation of exposures to ambient air pollution. *Journal of the Royal Statistical Society: Series C (Applied Statistics)* 67(1):231–253

Sklar M (1959) Fonctions de repartition an dimensions et leurs marges. *Publ inst statist univ Paris* 8:229–231

Song C, Wu L, Xie Y, He J, Chen X, Wang T, Lin Y, Jin T, Wang A, Liu Y, et al (2017) Air pollution in China: status and spatiotemporal variations. *Environmental pollution* 227:334–347

Wood S, Wood MS (2015) Package ‘mgcv’. R package version 1:29

World Health Organization (2013) Review of evidence on health aspects of air pollution—REVIHAAP Project. World Health Organization, Copenhagen, Denmark